Deep crustal contact between the Pamir and Tarim Basin deduced from receiver functions

Qiang Xu[1, 2], Junmeng Zhao[1, 2], Xiaohui Yuan[3], Hongbing Liu[1], Changhui Ju[1], Bernd Schurr[3], Wasja Bloch[3]

[1] Key Laboratory of Continental Collision and Plateau Uplift, Institute of Tibetan Plateau Research, Chinese Academy of Sciences, Beijing 100101, China

[2] CAS Center for Excellence in Tibetan Plateau Earth Sciences, Beijing 100101, China

[3] Deutsches GeoForschungsZentrum GFZ, Telegrafenberg, Potsdam 14473, Germany

[*]Corresponding authors: zhaojm@itpcas.ac.cn; xuqiang@itpcas.ac.cn

Key Points

· The Asian lower crust is delaminated beneath the central east Pamir

· The northeast Pamir crust extends into the Tarim Basin and thickens by pure shear shortening

· The southeast Pamir crust is underthrusting beneath West Kunlun Shan and Tarim Basin

Abstract

The deep crustal deformation in the east Pamir in response to Cenozoic collision with the Tien Shan and Tarim Basin is so far poorly constrained. We present new insights into the crustal structure of the east Pamir and the surrounding regions using P receiver functions from 40 temporary and permanent seismic stations. The crustal

thickness reaches a maximum of 88 km beneath the central and southern east Pamir and decreases sharply to 50-60 km along the southern Tien Shan and to 41-50 km below Tarim Basin. The most prominent crustal structures involve a double Moho and two Moho offsets, which suggest that the crustal deformation in the east Pamir is controlled by multiple mechanisms, including delamination of Asian lower crust below the central east Pamir, pure shear shortening along the northeastern margin between the Pamir and Tarim/Tien Shan and eastward underthrusting of Pamir lower crust beneath the southern east Pamir.

Plain Language Summary

The Pamir orogen is located at the leading edge of the Indo-Asian collision zone and has translated northward by about 300 km with respect to the Himalaya-Tibetan plateau since the Late Cenozoic. It protruded the formerly connected Tajik and Tarim basins and formed a curviplanar front with Tajik Basin to the west, Tien Shan to the north and Tarim Basin to the east. Previous studies revealed that the Pamir is underthrusted by the Asian crust from the west and from the north; however, it is still unclear how the contact between Pamir and the Tarim basin crust looks like. This study elucidates the deep crustal interaction between the two tectonic blocks by receiver functions with data from a recent seismic experiment in the region. The Pamir crust is extended into the western tip of the Tarim basin and is thickened by pure shear, while in the south it is subducted beneath the West Kunlun Shan and Tarim Basin into the mantle to a depth of >100 km.

Keywords: east Pamir, Tarim Basin, receiver functions, crustal structure, continental crust subduction, delamination

1. Introduction

The Pamir orogen lies north of the western Himalayan syntaxis in the India-Asia collision zone (Figure 1) and attains an elevation of ≥ 4 km and a crustal thickness of 65-75 km by absorbing ~55-64% Cenozoic shortening within a relatively narrow north-south distance compared to the main Tibetan Plateau (Schmidt et al., 2011). A major orocline has formed due to the northward displacement of the Pamir by at least 300 km relative to Tibet and the Hindu Kush, with bending of this orogen associated with several well-developed thrusting and strike-slip faults along its margins (Figure 1); these include the sinistral Darvaz-Karakul strike-slip fault bounding Tajik Basin to the west, the dextral Kashgar-Yecheng Transfer System (KYTS) bounding Tarim Basin to the east and the Main Pamir Thrust (MPT) bounding Alai Valley to the north (Figure 1). Structurally, the Pamir comprises a series of terranes that were accreted during the Paleozoic and Early Mesozoic. The Pamir can be divided into the North, Central and South Pamir, which are separated by the Tanymas and Rushan-Pshart sutures (Schwab et al., 2004).

Intense intermediate-depth seismicity has been observed beneath the Pamir and Hindu Kush (Sippl et al., 2013a), which is interpreted as evidence for ongoing

intracontinental subduction (Schneider et al., 2013; Sobel et al., 2013) or forced delamination(Kufner et al., 2016). The opposite dips of deep earthquakes beneath the Pamir and Hindu Kush have invoked different interpretations about the plate configuration ranging from a single contorted slab of Indian (Pavlis & Das, 2000), or Asian origin (Perry et al., 2019) to a two-slab model that involves the eastward to southward subduction/delamination of Asian lithosphere in a tight 90° arc beneath the Pamir and northward subduction of Indian lithosphere beneath the Hindu Kush (Kufner, et al., 2016; Negredo et al., 2007). A receiver function image along a north-south profile at ~73.8° E reveals that these intermediate-depth earthquakes occur in a 10 -15 km thick low velocity zone (LVZ) possibly associated with the southward subduction of Asian lower crust reaching a depth of 150 km (Schneider, et al., 2013), consistent with the results of local earthquake tomography and guided waves analyses (Mechie et al., 2019; Sippl et al., 2013b). Recently, an additional NW-SE trending intermediate-depth earthquake zone has been identified south of the eastern termination of E-W striking segment of the Pamir seismic zone, roughly parallel to the Karakax fault (KXF) (Bloch et al., 2020), which suggests a different and still ambiguous origin compared to the Pamir-Hindu Kush seismic zone.

A previous receiver function analysis shows a double Moho structure at 50-90 km depth, which hints at underthrusting of the Tajik lower crust beneath western Pamir (Schneider et al., 2019). Plate motion vectors and seismotectonic analysis testify that crustal materials flow outward from the interior of the Pamir towards the western

flanks and/or extrude upward along a series of thrust faults (Schurr et al., 2014). Conversely, the rigid Tarim crust may hinder eastward extrusion of the east Pamir (Metzger et al., 2020; Schurr, et al., 2014). The dextral KYTS as the boundary between the east Pamir and Tarim Basin is supposed to be the eastern edge of subducting Asian lithosphere (Sobel, et al., 2013). These studies provide no evidence for subduction of Tarim Basin beneath the east Pamir, but how the crust deforms in the east Pamir facing the obstruction of the Tarim Basin remains insufficiently constrained, partly due to limited data available in this region.

In this study, we use P receiver functions (PRFs) derived from a recently deployed temporary seismic array and permanent stations to investigate the crustal structure beneath the east Pamir and the adjacent region at a higher resolution than has previously been possible. Our crustal thickness and Vp/Vs ratio observations provide new insights into the crustal deformation patterns in the east Pamir under the resistance of Tarim Basin and Tien Shan during intracontinental orogenesis.

2. Data and methods

The three-component seismograms used in this study were recorded at 40 broadband stations during the period from 2015 to 2017, consisting of 31 stations in a temporary two-dimensional (2-D) seismic array of the east Pamir seismic experiment (FDSN code 8H; (Yuan et al., 2018)) and 9 permanent stations from China Earthquake Administration (CEA) network (Zheng et al., 2010) (Figure 1). We selected

111 teleseismic earthquakes with signal-to-noise ratios on the vertical component ≥2.5,
112 body-wave magnitudes (Mb) ≥5.5, and epicentral distances in the 30-95° range for the
113 PRF computations.
114
115 PRF analysis is one of the most frequently used techniques to explore the seismic
116 structures underneath a seismic station using the P-to-S (Ps) conversions and
117 associated multiples that originate from discontinuities at different depths. The raw
118 Z-N-E traces of each event are rotated into the ray-based P-SV-SH coordinate system
119 using the theoretical back azimuth and incident angle. The P component is then
120 deconvolved from the SV component using a time domain Wiener filtering method to
121 produce the SV receiver function (PRF) (Yuan et al., 1997). A visual quality control
122 was carried out on all of the PRFs to eliminate outliers with significant oscillations or
123 strong amplitudes. Finally, a total of 3153 PRFs, obtained from 270 teleseismic events,
124 were retained for subsequent processing.
125
126 We estimate the crustal thickness (H) and Vp/Vs ratio (κ) at each station using the
127 delay times of the Moho Ps and PpPs phases (Xu et al., 2017). This algorithm avoids
128 the effects of multiple extremes on the energy surface that are often confronted by the
129 popular H-κ stacking method in complex orogenic areas(Murodov et al., 2018; Zhu &
130 Kanamori, 2000), thereby yielding more robust solutions for H and κ. We manually
131 pick both delay times on two individual sum traces that are produced by stacking all
132 of the PRFs from each station after a moveout correction for the Ps and PpPs phases,

133 respectively. To identify the PpPs phase reliably, we pick this phase within a predicted
134 time window based on the picked delay time of the Moho Ps conversion and two κ
135 values of 1.6 and 2.0. The two standard deviations obtained using the bootstrap
136 resampling technique (Xu, et al., 2017), are considered as the uncertainties for both H
137 and κ (Table S1).
138
139 To delineate the morphology of the subsurface discontinuities, three cross sections are
140 constructed using a common conversion point (CCP) stacking technique (Yuan et al.,
141 2000). The amplitudes of each PRF are back projected along their ray paths to their
142 respective depths within a Fresnel zone around the piercing points. We perform the
143 ray tracing and time-depth conversion using a 2-D velocity model along each cross
144 section which is interpolated from the 1-D modified IASP91 model for each station,
145 whereby the crustal structure has been changed using the P wave velocity model from
146 a wide-angle reflection/refraction profile within the study area and the resulting
147 Vp/Vs ratio (Zhang et al., 2002). Especially, the revised 1-D model includes a 5 km
148 thick sedimentary layer with Vp = 3.20 km/s and Vs = 1.82 km/s for the stations at
149 <1.5 km elevation in Tarim Basin,
150
151 ## 3. Results
152 Figure 2 exhibits PRF stacks for 38 stations, together with the carefully picked delay
153 times of the Moho Ps and PpPs phases. The Moho Ps and PpPs conversions arrive at
154 5.3 to 11.5 s and 18.2 to 38.1 s, respectively. Stations KSH and EP16 (Figure S1) are

not included due to ambiguous Moho Ps signals caused by strong sedimentary reverberations. We simultaneously obtain H and κ values for 35 stations, for which both the Moho Ps and PpPs are clearly visible. For three other stations, we could not determine the κ values because the Moho PpPs phases are unclear. We only estimate the H values using the arrival times of the Moho Ps conversions and κ values from their adjacent stations (Table S1).

We generate a regional-scale crustal thickness map across the Pamir and the surrounding region by combining previously published results with the measurements obtained in this study (Table S2 and Figure 3a). Details of crustal thickness variations outside our study region can be found in Schneider et al. (2019) and Zhang et al. (2020). The map reveals two deep Moho regions (called Moho troughs), one in the western central Pamir along the boundary region of the Pamir with the Tajik basin (Schneider et al., 2019), the other in the east Pamir along the West Kunlun Shan, the boundary region with the Tarim basin. Both Moho troughs are parallel to intermediate-depth seismic zones. In this paper we focus on our observations in the east Pamir. The resulting H values decrease from 67-88 km beneath the east Pamir to 50-60 km along the southern Tien Shan and 41-50 km beneath the Tarim Basin. The thickest crust (up to 88 km) is observed in the southeastern Pamir along the West Kunlun Shan and an elongated region of thicker crust with a thickness ranging from 68 to 74 km in the northeastern margin of the Pamir extends northeastward to the Pamir Frontal Thrust (PFT). Figure 3b indicates that the κ values vary significantly,

ranging from 1.68 to 1.89 with an average uncertainty of 0.02. The low to moderate κ values of 1.68-1.81 are mainly distributed throughout the east Pamir, suggesting felsic and intermediate bulk crustal compositions possibly resulted from delamination or foundering of the mafic lower crust. The high κ values of more than 1.81 in Tarim Basin are likely caused by the thick sedimentary sequences, whereas those in the east Pamir and southern Tien Shan may be the result of fractured damage zones and/or partial melt within the crust.

Strong positive conversions at depths of 40-90 km, which are interpreted to be indicative of the Moho, are clearly identified in the CCP stacking images along three selected cross sections (Figure 4). Superimposing the crustal thicknesses over the three CCP images reveals a good agreement with the lateral variations in Moho depth, giving confidence that the imaged Moho structure is credible. A Moho offset of at least 12 km appears below the surface trace of the PFT along profile A-A', separating a sub-horizontal Moho at depths of 70-78 km in the south from a shallowly south-dipping Moho at 50-58 km depth in the north. A double Moho structure is observed below the surface trace of the KXF along profile B-B'; the deeper Moho reaches a depth of 88 km and continues to dip eastward, while the shallower Moho at depths of 62-66 km gradually shallows to 45 km beneath Tarim Basin. The individual PRFs at stations EP27 and EP30 (Figure S1) which are located above this double structure are shown in Figure S2. Profile C-C' is characterized by another significant Moho offset of about 18 km below Muztagh Ata (MA); this offset separates a

south-dipping Moho at 60-88 km depth in the north from a sub-horizontal Moho at 70-78 km depth in the south.

We generate the maps of the hit counts at each bin of the CCP stacks along three cross sections (Figure S3). The hit count represents the PRF ray coverage beneath each profile. The ray coverage of our imaged Moho structure is quite good with hit counts more than 100, which suggests that the distinguishing features of Moho described above is reliable.

4. Discussion

The most striking features observed in our CCP stacking images are the presence of a double Moho structure and two Moho offsets, which contribute fresh insights into the dynamic processes of crustal deformation in the east Pamir and the surrounding region. Figure 5 summarizes our structural interpretation of the imaged crustal structure.

The Moho offset observed below the PFT in northeastern (NE) Pamir marks the tectonic boundary between the Pamir and the Tarim Basin. Under the regional tectonic settings of the northward indentation of the Pamir and the resistance of the strong Tarim lithosphere, the development of the Moho offset suggests that pure shear shortening is responsible for the crustal thickening in the NE Pamir. This interpretation is consistent with stratigraphic and magnetostratigraphic data,

suggesting that the PFT became the leading edge of the Pamir deformation around 5-6 Ma and accommodated the Quaternary shortening along the NE margin of the Pamir (Thompson et al., 2015). Analogous scenarios have also been reported in the transitional regions between the South-Central Tien Shan and northern Tarim Basin (Zhang et al., 2020), and along the boundary between western Tibet and the southern Tarim Basin (Murodov, et al., 2018). Furthermore, a similar Moho offset is inconspicuous in the North Pamir-Tien shan collision zone, which is west of the elongated region of thicker crust. The reasons for this phenomenon could be that the lithospheric strength of Tien shan is weaker than that beneath Tarim Basin (Bagdassarov et al., 2011), and much of the shortening between North Pamir and the southern Tien Shan has migrated into the Tien Shan east of 75°E since 10 Ma (Sobel et al., 2006).

Previous studies have demonstrated the delamination of Asian lower crust beneath North and Central Pamir west of our study area (Schneider et al., 2013; Kufner, et al., 2016). Following these studies and considering the dominant E-W distribution of intermediate-depth seismicity, we suggest that the Moho offset observed beneath MA represents the eastward expansion of the delaminated Asian lower crust terminating at the KYTS. This scenario of no overlapping Moho and sinking Asian lower crust is in more accordance with delamination than classical subduction (Bird, 1979), because the downgoing Asian crust is primarily driven by the indentation of Indian lithosphere and negative buoyancy due to the eclogitization of Asian lower crust (Schneider et al.,

2013; Kufner, et al., 2016). Alternatively, large-scale asthenospheric flow, which has been inferred from shear wave splitting measurements, may have also delivered relatively hot materials into the crust through a crustal tear between Tarim Basin and the Asian lithosphere, possibly facilitating the delamination of Asian lower crust (Bird, 1979; Kufner et al., 2018). Decompression- and dehydration-related melts that form following the delamination of eclogitized crust and mantle lithosphere can intrude upward into the middle and lower crust. These intrusions can cause crustal anatexis, which is thought to have contributed to rapid exhumation of the Muztagh Ata and Kongur Shan domes, which are possibly associated with successive stages of delamination of the Asian lithosphere (Li et al., 2020; Thiede et al., 2013).

The most intriguing structure of our observations is a double Moho in the southern portion of the east Pamir. In conjunction with the NW-SE trending intermediate-depth seismicity, we suggest that this double Moho structure provides direct evidence for eastward underthrusting of the Pamir lower crust beneath the West Kunlun Shan and Tarim Basin. Conversely, a similar structure identified below western Pamir has been interpreted to represent underthrusting of the Tajik lower crust (Schneider, et al., 2019). The spatial relationship of the two Moho troughs with the intermediate-depth seismic zones implies that underthrusting involves crust. In the west Pamir, the Moho trough is located northwest of the seismic zone, suggesting a southeastward underthrusting of the Asian crust (Schneider, et al., 2019). In the east Pamir, the Moho trough is to the west of the seismic zone, indicating an eastward underthrusting of the

Pamir crust. Our interpretation is compatible with sedimentary and magnetostratigraphic analyses along the Aertashi section, which indicate eastward-directed thrusting of the Pamir onto Tarim Basin and an rotation from approximately N-S to E-W in the maximum strain orientation at 15 Ma (Blayney et al., 2019). Crustal xenoliths from the Dunkeldik volcanic field erupted at ~11 Ma in the southeastern Pamir suggest that Gondwanan Pamir crust was subducted to depths of 90-100 km beneath Eurasia (Hacker et al., 2005), which is analogous to our interpretation. A notable high-velocity anomaly imaged below 180 km depth has been interpreted as northward underthrusting Indian mantle lithosphere (Li et al., 2008), which may provide the driving force for the development of the underthrusting structure described here.

5. Conclusions

We obtain the crustal structure below the east Pamir and the adjacent region by applying PRF techniques to teleseismic waveforms recorded at a temporary 2-D seismic array and the permanent stations. The crustal thickness ranges from 67-88 km beneath the east Pamir and reduces to 50-60 km along the southern Tien Shan and 41-50 km in the Tarim basin. Our depth migration images indicate the presence of a double Moho structure and two Moho offsets, which shed new light on crustal deformation patterns in the east Pamir. We suggest that pure shear shortening accounts for crustal thickening in NE Pamir, while delamination of Asian lower crust and eastward underthrusting of Pamir lower crust dominate the deformation processes in

the central and southern portions of the east Pamir, respectively.

Acknowledgments

This research was funded by the Strategic Priority Research Program of Chinese Academy of Sciences (Grant No. XDA20070302) and the CaTeNA project of the German Federal Ministry of Science and Education (support code 03G0878A). The temporary seismic experiment (8H) was partly supported by the expedition fund from Deutsches GeoForschungsZentrum GFZ. Temporary instruments were provided by the Geophysical Instrument Pool Potsdam (GIPP). Seismic data are archived at the GEOFON data center (Yuan, et al., 2018) and at the Institute of Tibetan Plateau Research, Chinese Academy of Sciences. We thank the Data Management Centre of the China National Seismic Network at the Institute of Geophysics, China Earthquake Administration, for providing waveform data of permanent stations (SEISDMC, doi:10.11998/SeisDmc/SN, http://www.seisdmc.ac.cn/; Zheng et al., 2010).

References

Bagdassarov, N., Batalev, V., & Egorova, V. (2011). State of lithosphere beneath Tien Shan from petrology and electrical conductivity of xenoliths. *Journal of Geophysical Research-Solid Earth, 116,* B01202. https://doi.org/10.1029/2009jb007125

Bird, P. (1979). Continental Delamination and the Colorado Plateau. *Journal of Geophysical Research, 84*(B13), 7561-7571.

https://doi.org/10.1029/Jb084ib13p07561

Blayney, T., Dupont-Nivet, G., Najman, Y., Proust, J. N., Meijer, N., Roperch, P. (2019). Tectonic Evolution of the Pamir Recorded in the Western Tarim Basin (China): Sedimentologic and Magnetostratigraphic Analyses of the Aertashi Section. *Tectonics, 38*(2), 492-515. https://doi.org/10.1029/2018TC005146

Bloch, W., Schurr, B., Yuan, X., Ratschbacher, L., Abdulhameed, A, Kufner, S.-K., Xu, Q., Zhao, J. (2020). Structure of the deep lithosphere between Pamir and Tarim, *Geology* (submitted).

Hacker, B., Luffi, P., Lutkov, V., Minaev, V., Ratschbacher, L., Plank, T. (2005). Near-ultrahigh pressure processing of continental crust: Miocene crustal xenoliths from the Pamir. *Journal of Petrology, 46*(8), 1661-1687. https://doi.org/10.1093/petrology/egi030

Kufner, S. K., Eken, T., Tilmann, F., Schurr, B., Yuan, X. H., Mechie, J. (2018). Seismic Anisotropy Beneath the Pamir and the Hindu Kush: Evidence for Contributions From Crust, Mantle Lithosphere, and Asthenosphere. *Journal of Geophysical Research-Solid Earth, 123*(12), 10727-10748. https://doi.org/10.1029/2018JB015926

Kufner, S. K., Schurr, B., Sippl, C., Yuan, X. H., Ratschbacher, L., Akbar, A. S. M. (2016). Deep India meets deep Asia: Lithospheric indentation, delamination and break-off under Pamir and Hindu Kush (Central Asia). *Earth and Planetary Science Letters, 435*, 171-184. https://doi.org/10.1016/j.epsl.2015.11.046

Li, C., Van der Hilst, R. D., Meltzer, A. S., & Engdahl, E. R. (2008). Subduction of the Indian lithosphere beneath the Tibetan Plateau and Burma. *Earth and Planetary Science Letters*, *274*(1-2), 157-168. https://doi.org/10.1016/j.epsl.2008.07.016

Li, Y. P., Robinson, A. C., Lapen, T. J., Righter, M., & Stevens, M. K. (2020). Muztaghata Dome Miocene Eclogite Facies Metamorphism: A Record of Lower Crustal Evolution of the NE Pamir. *Tectonics, 39*, e2019TC005917. https://doi.org/10.1029/2019TC005917

Mechie, J., Schurr, B., Yuan, X., Schneider, F., Sippl, C., Minaev, V. (2019). Observations of guided waves from the Pamir seismic zone provide additional evidence for the existence of subducted continental lower crust. *Tectonophysics, 762*, 1-16. https://doi.org/10.1016/j.tecto.2019.04.007

Metzger, S., Ischuk, A., Deng, Z., Ratschbacher, L., Perry, M., Kufner, S. K. (2020). Dense GNSS Profiles Across the Northwestern Tip of the India‐Asia Collision Zone: Triggered Slip and Westward Flow of the Peter the First Range, Pamir, Into the Tajik Depression. *Tectonics, 39*(2), e2019TC005797. https://doi.org/10.1029/2019TC005797

Murodov, D., Zhao, J. M., Xu, Q., Liu, H. B., & Pei, S. P. (2018). Complex N-S variations in Moho depth and V (p)/V (s) ratio beneath the western Tibetan Plateau as revealed by receiver function analysis. *Geophysical Journal International*, *214*(2), 895-906. https://doi.org/10.1093/gji/ggy170

Negredo, A. M., Replumaz, A., Villasenor, A., & Guillot, S. (2007). Modeling the

353 evolution of continental subduction processes in the Pamir-Hindu Kush region.
354 *Earth and Planetary Science Letters, 259*(1-2), 212-225.
355 https://doi.org/10.1016/j.epsl.2007.04.043
356 Pavlis, G. L., & Das, S. (2000). The Pamir-Hindu Kush seismic zone as a strain
357 marker for flow in the upper mantle. *Tectonics, 19*(1), 103-115.
358 https://doi.org/10.1029/1999tc900062
359 Perry, M., Kakar, N., Ischuk, A., Metzger, S., Bendick, R., Molnar, P. (2019). Little
360 Geodetic Evidence for Localized Indian Subduction in the Pamir-Hindu Kush
361 of Central Asia. *Geophysical Research Letters, 46*(1), 109-118.
362 https://doi.org/10.1029/2018GL080065
363 Schmidt, J., Hacker, B. R., Ratschbacher, L., Stubner, K., Stearns, M., Kylander-Clark,
364 A. (2011). Cenozoic deep crust in the Pamir. *Earth and Planetary Science*
365 *Letters, 312*(3-4), 411-421. https://doi.org/10.1016/j.epsl.2011.10.034
366 Schneider, F. M., Yuan, X., Schurr, B., Mechie, J., Sippl, C., Haberland, C. (2013).
367 Seismic imaging of subducting continental lower crust beneath the Pamir.
368 *Earth and Planetary Science Letters, 375*, 101-112.
369 https://doi.org/10.1016/j.epsl.2013.05.015
370 Schneider, F. M., Yuan, X., Schurr, B., Mechie, J., Sippl, C., Kufner, S. K. (2019). The
371 Crust in the Pamir: Insights From Receiver Functions. *Journal of Geophysical*
372 *Research-Solid Earth, 124*(8), 9313-9331.
373 https://doi.org/10.1029/2019JB017765
374 Schurr, B., Ratschbacher, L., Sippl, C., Gloaguen, R., Yuan, X. H., & Mechie, J.

(2014). Seismotectonics of the Pamir. *Tectonics, 33*(8), 1501-1518. https://doi.org/10.1002/2014TC003576

Schwab, M., Ratschbacher, L., Siebel, W., Williams, M. M., Minaev, V., Lutkov, V. (2004). Assembly of the Pamirs: Age and origin of magmatic belts from the southern Tien Shan to the southern Pamirs and their relation to Tibet. *Tectonics, 23*(4), TC4002. https://doi.org/10.1029/2003TC001583

Sippl, C., Schurr, B., Yuan, X., Mechie, J., Schneider, F. M., Gadoev, M. (2013a). Geometry of the Pamir-Hindu Kush intermediate-depth earthquake zone from local seismic data. *Journal of Geophysical Research-Solid Earth, 118*(4), 1438-1457. https://doi.org/10.1002/jgrb.50128

Sippl, C., Schurr, B., Tympel, J., Angiboust, S., Mechie, J., Yuan, X. (2013b). Deep burial of Asian continental crust beneath the Pamir imaged with local earthquake tomography. *Earth and Planetary Science Letters, 384*, 165-177. https://doi.org/10.1016/j.epsl.2013.10.013

Sobel, E. R., Chen, J., & Heermance, R. V. (2006). Late Oligocene-Early Miocene initiation of shortening in the Southwestern Chinese Tian Shan: Implications for Neogene shortening rate variations. *Earth and Planetary Science Letters, 247*(1-2), 70-81. https://doi.org/10.1016/j.epsl.2006.03.048

Sobel, E. R., Chen, J., Schoenbohm, L. M., Thiede, R., Stockli, D. F., Sudo, M. (2013). Oceanic-style subduction controls late Cenozoic deformation of the Northern Pamir orogen. *Earth and Planetary Science Letters, 363*, 204-218. https://doi.org/10.1016/j.epsl.2012.12.009

Thiede, R. C., Sobel, E. R., Chen, J., Schoenbohm, L. M., Stockli, D. F., Sudo, M. (2013). Late Cenozoic extension and crustal doming in the India-Eurasia collision zone: New thermochronologic constraints from the NE Chinese Pamir. *Tectonics, 32*(3), 763-779. https://doi.org/10.1002/tect.20050

Thompson, J. A., Burbank, D. W., Li, T., Chen, J., & Bookhagen, B. (2015). Late Miocene northward propagation of the northeast Pamir thrust system, northwest China. *Tectonics, 34*(3), 510-534. https://doi.org/10.1002/2014TC003690

Xu, Q., Zhao, J. M., Yuan, X. H., Liu, H. B., & Pei, S. P. (2017). Detailed Configuration of the Underthrusting Indian Lithosphere Beneath Western Tibet Revealed by Receiver Function Images. *Journal of Geophysical Research-Solid Earth, 122*(10), 8257-8269. https://doi.org/10.1002/2017JB014490

Yuan, X., Schurr, B., Bloch, W., Xu, Q., & Zhao, J. (2018). The 8H East Pamir seismic network. *GFZ Data Services*. https://doi.org/10.14470/3U7560589977

Yuan, X., Sobolev, S. V., Kind, R., Oncken, O., Bock, G., Asch, G. (2000). Subduction and collision processes in the Central Andes constrained by converted seismic phases. *Nature, 408*(6815), 958-961

Yuan, X. H., Ni, J., Kind, R., Mechie, J., & Sandvol, E. (1997). Lithospheric and upper mantle structure of southern Tibet from a seismological passive source experiment. *Journal of Geophysical Research-Solid Earth, 102*(B12), 27491-27500. https://doi.org/10.1029/97jb02379

Zhang, B. F., Bao, X. W., & Xu, Y. X. (2020). Distinct Orogenic Processes in the South- and North-Central Tien Shan From Receiver Functions. *Geophysical Research Letters*, *47*(6), e2019GL086941. https://doi.org/10.1029/2019GL086941

Zhang, X. K., Zhao, J. R., Zhang, C. K., Ren, Q. F., Nie, W. Y., Cheng, S. X. (2002). Crustal structure at the northeast side of the Pamirs. *Chinese Journal of Geophysics-Chinese Edition, 45*(5), 665-671

Zheng, X. F., Yao, Z. X., Liang, J. H., & Zheng, J. (2010). The Role Played and Opportunities Provided by IGP DMC of China National Seismic Network in Wenchuan Earthquake Disaster Relief and Researches. *Bulletin of the Seismological Society of America*, *100*(5B), 2866-2872. https://doi.org/10.1785/0120090257

Zhu, L., & Kanamori, H. (2000). Moho depth variation in southern California from teleseismic receiver functions. *Journal of Geophysical Research: Solid Earth, 105*(B2), 2969-2980. https://doi.org/10.1029/1999JB900322

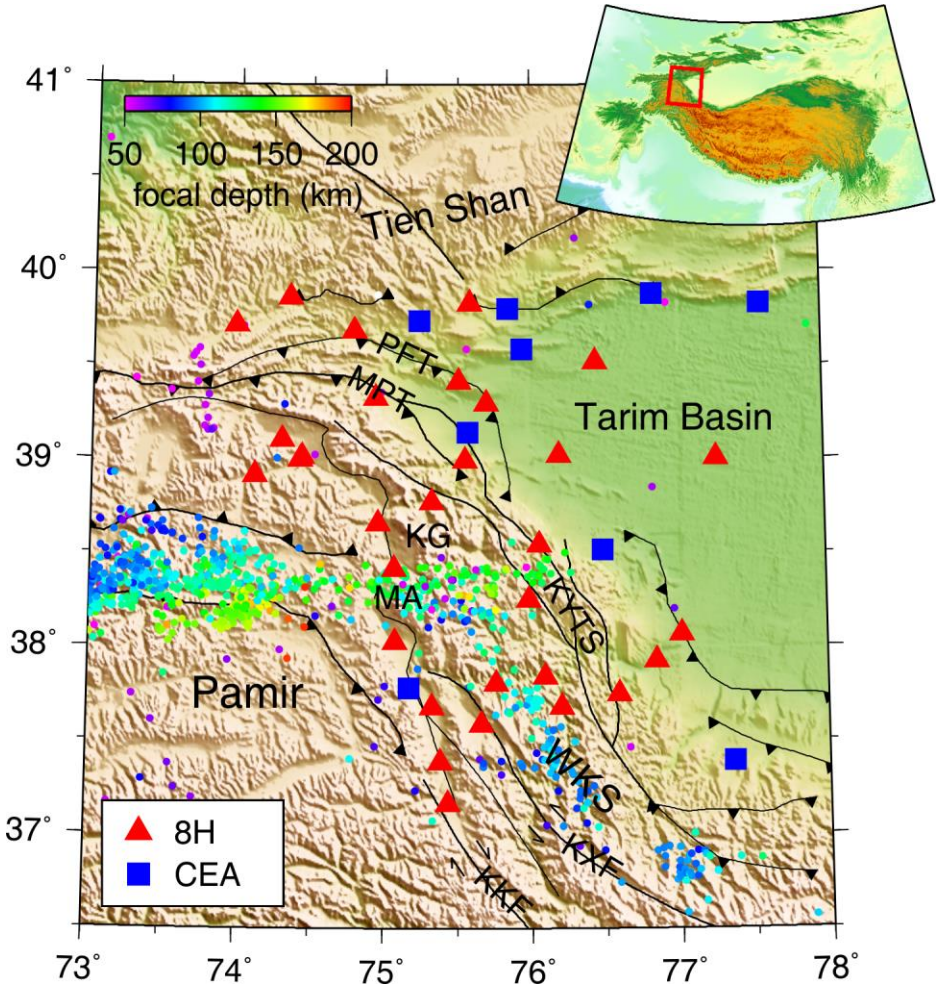

Figure 1. Topographic map of East Pamir showing simplified faults and locations of the seismic stations. The red triangles represent 8H stations, and the blue squares denote the CEA permanent stations. The color-coded dots mark the intermediate-depth earthquakes at depths greater than 50 km from Bloch et al. (2020). The top right inset illustrates the location of our study region (red box) relative to the India-Asia collision zone. Abbreviations are as follows: MPT, Main Pamir Thrust; PFT, Pamir Frontal Thrust; KYTS, Kashgar-Yecheng Transfer System; KKF, Karakoram fault; KXF, Karakax fault; MA, Muztagh Ata; KG, Kongur Shan; WKS, West Kunlun Shan.

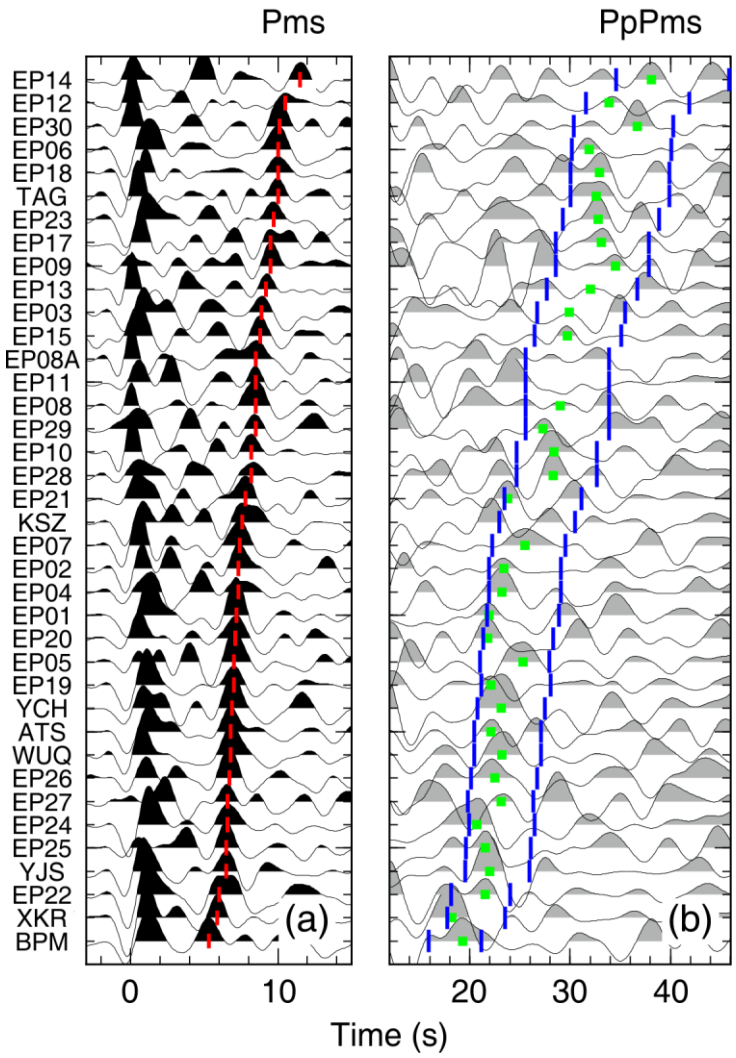

Figure 2. Stacks of PRFs for each station with moveout corrections already completed for (a) Ps and (b) PpPs sorted by the delay time of the Moho Ps conversion. The red ticks and green squares delineate the picked arrivals of the Moho Ps and PpPs phases, respectively. The blue ticks mark the predicted time windows for the appearance of the PpPms phase at each station.

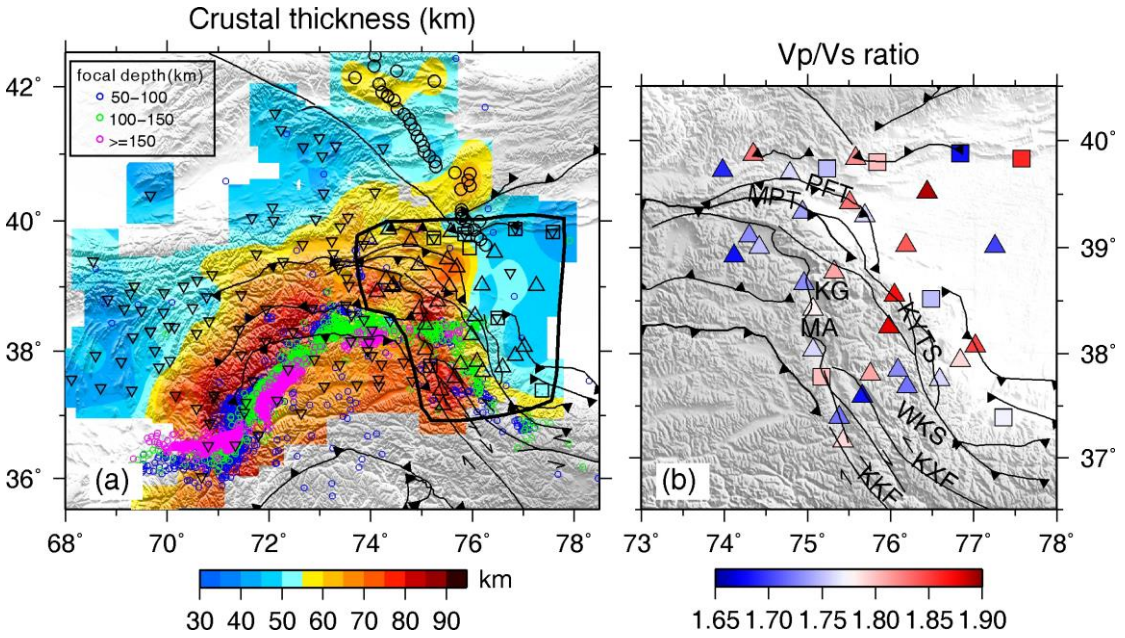

Figure 3. Maps of the (a) crustal thickness and (b) average Vp/Vs ratio. The crustal thickness values from Schneider et al. (2019) and Zhang et al. (2020) have also been included in Figure 3a. The intermediate-depth earthquakes at depths greater than 50 km from Bloch et al. (2020) are marked in Figure 3a by color-coded circles. The results for the area delineated by the black line in Figure 3a are analyzed in detail in this study.

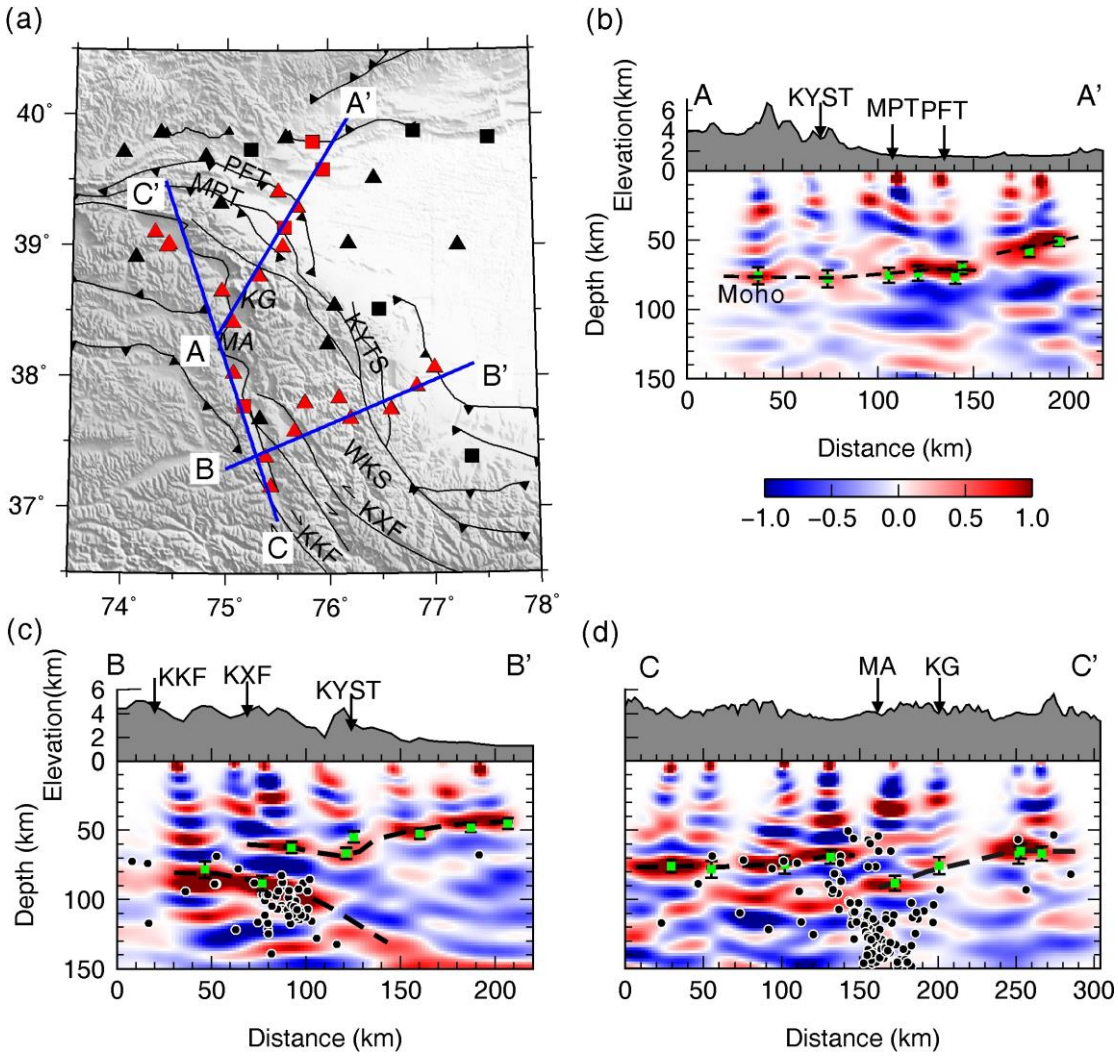

Figure 4. CCP stacking images along three cross sections, A-A', B-B' and C-C'. The positive (negative) amplitudes are filled in red (blue) to indicate the interfaces where the velocity increases (decreases) with depth. The resulting crustal thicknesses and errors are marked by the green squares and bars, respectively, and are superimposed on the well-resolved Moho conversions (black dashed lines). The black circles are the projected intermediate-depth earthquakes perpendicular to the profile within 50 km. The top left panel shows the locations of cross sections. Stations used in the three CCP cross sections are marked by red color.

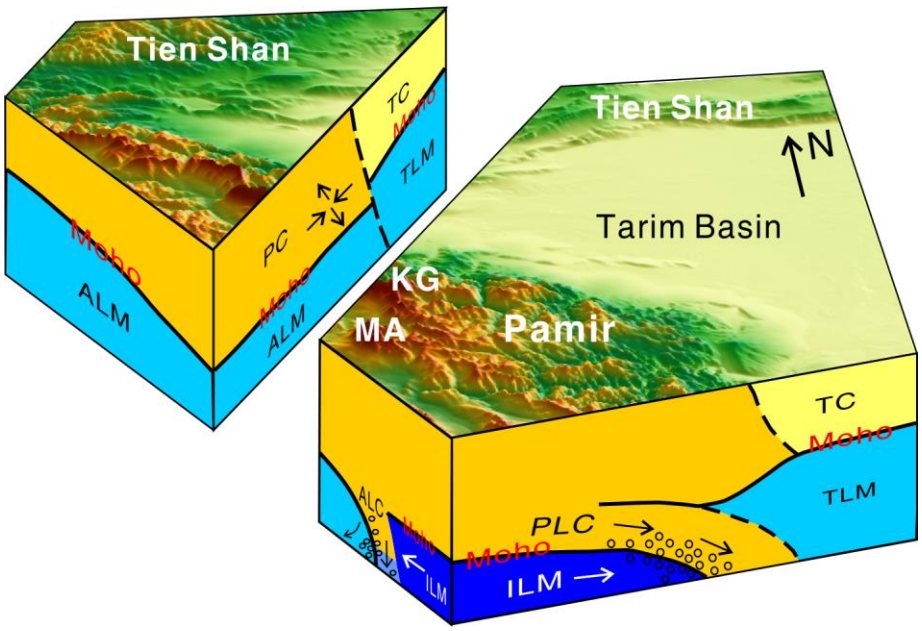

Figure 5. 3-D schematic illustration for the proposed deformation patterns beneath the east Pamir. The black circles are the symbolic intermediate-depth earthquakes. Abbreviations are as follows: ILM, Indian lithospheric mantle; PC, Pamir crust; PLC, Pamir lower crust; ALC, Asian lower crust; ALM, Asian lithospheric mantle; TC, Tarim crust; TLM, Tarim lithospheric mantle.